Available online at www.sciencedirect.com

ScienceDirect

Advances in Space Research 77 (2026) 671–685

ADVANCES IN SPACE RESEARCH (a COSPAR publication)

www.elsevier.com/locate/asr

Nonlinear formation tracking control based on generalized canonical transformations with adaptive mechanism for atmospheric drag

Satoshi Satoh *, Yuki Hamanaka

The University of Osaka, 2-1, Yamadaoka, Suita, Osaka 565-0871, Japan

Received 7 January 2025; received in revised form 10 October 2025; accepted 7 November 2025
Available online 15 November 2025

Abstract

This paper proposes a nonlinear formation tracking control method using generalized canonical transformations with an adaptive mechanism for atmospheric drag. This method theoretically guarantees that satellites asymptotically track given reference trajectories in formation flying under disturbances, including atmospheric drag and the gravitational J2 effect. First, the nonlinear relative orbital motion is modeled in a port-Hamiltonian system. Second, a specific transformation is constructed for any twice differentiable reference formation trajectory that converts the system into an error system in the form of a time-varying passive port-Hamiltonian system based on generalized canonical transformations. Third, a passivity-based asymptotic stabilizing controller and an adaptive mechanism for the error system are presented, provided that the atmospheric drag coefficient is an unknown constant. Overall, the proposed method guarantees that the estimation error of the atmospheric drag coefficient is bounded and that the tracking error for the reference trajectory converges uniformly asymptotically to zero.

Keywords: Adaptive control; Formation flying; Formation tracking control; Generalized canonical transformations; Port-Hamiltonian systems

1. Introduction

Formation flying (FF) (Alfriend et al., 2010; Mauro et al., 2018; Scharf et al., 2004) is a technology that distributes functions to multiple satellites, which fly in coordination while controlling their relative positions and attitudes. Various missions using FF have been proposed in recent years because FF enables missions that are difficult to achieve with a single large satellite due to physical limitations such as satellite size and weight. Examples of FF missions include the space gravitational wave telescope, LISA (Danzmann and Rüdiger, 2003; Xie et al., 2024) and DECIGO (Kawamura, 2008) and the infrared space interferometer, SEIRIOS (Matsuo et al., 2022) and LIFE (Quanz et al., 2022). The ongoing PROBA-3 mission (Llorente et al., 2013) launched in 2024 is a demonstrator of precise FF, which enables observation of the Sun's corona through the creation of an artificial solar eclipse. In May 2025, it successfully performed its first in-orbit demonstration (Serrano et al., 2025). In Ref. (Ito, 2024), the usefulness of the near-circular low Earth orbit (LEO) as an environment for in-orbit verification of FF technology was thoroughly investigated, where the relationship between the altitude and satellite relative distance for a small relative perturbation environment is exhibited. Due to their economical and feasible access, FF missions in LEO using low-cost nano-satellites have also been planned, e.g., (Molina et al., 2024). In addition, the ultra-precision FF technology demonstration project SILVIA has been proposed to acquire technologies that can be commonly

* Corresponding author.

https://doi.org/10.1016/j.asr.2025.11.031
0273-1177/

Nomenclature

t	time [s]
x	$n \times 1$ vector representing the state of the system
u	$m \times 1$ vector representing the control input
y	$m \times 1$ vector representing the output
H	Hamiltonian
$\mathscr{L}$	Lagrangian
$\mathscr{U}$	gravitational potential function including the J2 term
J	$n \times n$ skew-symmetric matrix representing the structure matrix
R_D	$n \times n$ positive semi-definite symmetric matrix representing the dissipation matrix
g	$n \times m$ matrix representing the control port
$\bar{x}$	$n \times 1$ vector representing the transformed state of the error system
$\overline{H}$	transformed Hamiltonian
$\bar{y}$	$m \times 1$ vector representing the transformed output
$\bar{u}$	$m \times 1$ vector representing the transformed control input
Φ	coordinate transformation: $\mathbb{R}^n \times \mathbb{R} \to \mathbb{R}^n$
U	Hamiltonian transformation: $\mathbb{R}^n \times \mathbb{R} \to \mathbb{R}$
α	output transformation: $\mathbb{R}^n \times \mathbb{R} \to \mathbb{R}^m$
β	input transformation: $\mathbb{R}^n \times \mathbb{R} \to \mathbb{R}^m$
Q	3×1 vector representing the position of the deputy in the ECI frame
q	3×1 vector representing the relative position of the deputy in the LVLH frame
q^d	3×1 vector representing a reference relative position in the LVLH frame
T	transformation matrix from the LVLH frame to the ECI frame
ω	3×1 vector representing the angular velocity of the LVLH frame to the ECI frame
p	3×1 vector representing the conjugate momentum of the deputy in the LVLH frame
μ	gravitational constant of the Earth [m^3/s^2]
R_e	radius of the Earth [m]
J_2	J2 coefficient
a	semi-major axis [m]
i	inclination [rad]
Ω	right ascension of the ascending node [rad]
θ	argument of latitude [rad]
n_c	mean motion of the chief [rad/s]
ρ_a	atmospheric density [kg/m^3]
A_C	effective area of a satellite [m^2]
C_D	drag coefficient
m_d	satellite mass [kg]
r_{Drag}	atmospheric drag coefficient
$\overline{R}_D$	$m \times m$ atmospheric drag matrix
$\hat{r}_{Drag}$	estimated atmospheric drag coefficient
$\widehat{R}_D$	$m \times m$ estimated atmospheric drag matrix
$\tilde{r}_{\mathrm{Drag}}$	$\hat{r}_{\mathrm{Drag}} - r_{\mathrm{Drag}}$, estimation error

Subscripts

c	chief satellite

Superscripts

$\top$	transpose
$^\times$	skew-symmetric matrix with dimension 3×3 representing the vector product

used for various future FF missions (Ito et al., 2025). The relative orbital motion between satellites, which is fundamental to FF, is governed by a nonlinear equation of motion. The Clohessy-Wiltshire equations (Clohessy and Wiltshire, 1960), or Hill's equations (Hill, 1878) obtained by linear approximation of the relative orbital motion, are useful in proximity maneuvers such as autonomous rendezvous and docking, e.g., JAXA's ETS-VII (Ohkami and Kawano, 2003) as an FF of practical importance. However, control methods that handle nonlinearity are essential for long-distance and ultra-precise formations, which are examined in the aforementioned future space interferometer observations.

Sliding mode control (Itkis, 1976; Shtessel et al., 2013) is a nonlinear control method suitable for on-board computation without iterative calculations and is expected to have high control performance and robustness. In Ref. (Li et al., 2018), a control method for rendezvous and docking was proposed that combines the artificial potential function method with a first-order sliding mode control. This method has the advantage of simultaneous collision avoidance and rendezvous and docking control under external disturbances. In Ref. (Bassetto et al., 2024), an active control method of drag sails for effective deorbit of LEO spacecraft is proposed based on sliding mode control. The proposed method maintains the sail surface normal in the direction of the velocity vector to maximize the passive drag effect under orbital and attitude perturbations. Although these methods both achieve control objectives and robustness against disturbances, a chattering phenomenon peculiar to the first-order sliding mode control is observed. Higher-order sliding mode control and terminal sliding mode control have been proposed to prevent chattering. In Refs. (Hui and Li, 2009; Lawn et al., 2018), agile formation control methods under disturbances based on robustness and finite-time convergence with terminal sliding mode control are proposed. The convergence rate of the terminal sliding mode control increases exponentially as the state approaches the target equilibrium point, and thus, fast convergence is achieved. However,

to realize such behavior on the sliding mode manifold, these methods need to cancel the original dynamics of the plant system significantly and to choose the design parameters carefully.

In contrast, controller design methodologies based on Hamiltonian systems and their generalizations, port-Hamiltonian systems (Maschke and van der Schaft, 1992; van der Schaft, 1996; Duindam et al., 2009), have been promising in controlling a broad class of practically important nonlinear systems. A significant advantage is that the energy shaping and dissipation can be explicitly considered because the Hamiltonian, the total energy of the system, and the interconnection and damping structures of the system explicitly appear in the system dynamics. This allows for energy-efficient control without unnecessarily canceling the system dynamics because a desired equilibrium point corresponding to the bottom of the potential can be easily set, and only factors causing energy increase need to be compensated. In addition, since the Hamiltonian is a Lyapunov function candidate, stability analysis for the resultant closed-loop system is also facilitated. In Ref. (Scheeres et al., 2003), a Hamiltonian-structure-preserving (HSP) controller is proposed to stabilize the relative motion to a libration point orbit. This method is also extended to the time-dependent relative dynamics in (Fu and Xu, 2019). The HSP control method utilizes the eigenstructure of the linearized relative dynamics along the target orbit, which compensates for the projected relative position along the directions of the stable and unstable manifolds of the linearized relative motion. This method has the advantage of stabilizing relative motions using only information on the relative position; however, controller design and stability analysis are based on the linearized relative dynamics and cannot directly handle nonlinearities of the relative orbital motions that are essential for the aforementioned long-distance formation and ultra-precise formation. The HSP control method can be interpreted as shaping the potential of a linearized Hamiltonian system. More generally, systematic methods that transform interconnection and damping structures as well as energy shaping while preserving the port-Hamiltonian structure include IDA-PBC method (Acosta et al., 2005; Ortega et al., 2002), generalized canonical transformations (Fujimito et al., 2003; Fujimito and Sugie, 2001), and kinetic potential energy shaping (KPES) method (Ferguson et al., 2019). In Ref. (Javanmardi et al., 2020), a trajectory tracking control of nonlinear relative orbital motions based on the IDA-PBC method is proposed. The IDA-PBC method provides an input transformation to a given target model of a port-Hamiltonian system with ideal closed-loop characteristics if the so-called matching condition is satisfied. However, the controller design of this method for complex systems is sometimes difficult in that the control performance and transformation should be simultaneously achieved.

In contrast, the main contributions of this paper are four folds:

1. A port-Hamiltonian representation of the nonlinear relative orbital motion with the gravitational J2 and atmospheric drag effects;
2. A concrete construction of an error system for a given reference formation trajectory using generalized canonical transformations;
3. An adaptive mechanism for an unknown atmospheric drag coefficient; and
4. An asymptotic formation tracking controller that stabilizes the error system based on its passivity.

Since the present method can divide the construction of the error system and its stabilization processes, it offers good prospects and flexibility in controller design for asymptotic formation tracking. For the first contribution, we represent the nonlinear relative orbital motion with the gravitational J2 effect, which is the gravitational perturbation due to the oblateness of the Earth, and the atmospheric drag in a port-Hamiltonian system with an additional disturbance term. According to Ref. (Ito et al., 2021), the gravitational J2 effect and the atmospheric drag are the first and second most significant environmental disturbances for the FF in a low Earth orbit. For the second contribution, we provide a specific generalized canonical transformation that transforms the nonlinear relative orbital motion into an error system in the form of a time-varying passive port-Hamiltonian system for any twice differentiable reference formation trajectories. For the third contribution, we propose an adaptive mechanism to estimate the coefficient, provided that the atmospheric drag coefficient is an unknown constant. Finally, a formation tracking controller is presented by stabilizing the error system using its passivity and the adaptive mechanism. The proposed method guarantees that the estimation error of the atmospheric drag coefficient is bounded, and the tracking error for the reference trajectory converges uniformly asymptotically to zero. From feature (1) and the main theorems described later (Theorems 2 and 3), the proposed method can handle any differentiable potential functions; hence, higher-order gravitational perturbations other than the J2 term and those from other celestial bodies can easily be involved. From feature (2) and the main theorems, the proposed method can also handle arbitrary twice differentiable reference trajectories; hence, not only various formation trajectories but also escape trajectories in an emergency can be handled in a unified manner. Since the proposed method is nonlinear formation control without requiring any linear approximations that are imposed in the conventional methods based on Hill's solutions or relative orbital elements (Alfriend et al., 2010; D'Amico and Montenbruck, 2006; Schaub and Junkins, 2018), it can be applied to long-distance and ultra-precise formations necessary for future formation flying space interferometer missions. In addition, the proposed controller is scalable independent of the number of satellites, because it does not require information from other satellites.

Preliminary reports of this paper appeared as conference papers (Hamanaka and Satoh, 2023; Satoh, 2021) without proofs, while the present paper unifies these results and provides detailed proofs for all lemmas and theorems. Besides, as a possible linkage between the sliding mode control and the proposed framework, one of the authors recently reported an application of a sliding mode controller to stabilize the error system aiming at higher robustness and convergence accuracy in (Tabuchi et al., 2022). This was accomplished by the separation of construction and stabilization of the error system in the proposed framework.

2. Preliminaries

This section defines the plant system considered in this paper and introduces transformations preserving the system structure, which play an important role in the subsequent controller design.

2.1. Port-Hamiltonian systems

A port-Hamilton system (Maschke and van der Schaft, 1992; van der Schaft, 1996; Duindam et al., 2009) is represented by the following equation:

$$\begin{cases} \dot{x} = (J(x,t) - R_D(x,t))\frac{\partial H(x,t)}{\partial x}^\top + g(x,t)u, \ x(0) = x_0 \\ y = g(x,t)^\top \frac{\partial H(x,t)}{\partial x}^\top \end{cases}, \quad (1)$$

where $x(t) \in \mathbb{R}^n$ and $u(t) \in \mathbb{R}^m$ denote the state and the control input, respectively. $y(t) \in \mathbb{R}^m$ is defined as a passive output to the system. The Hamiltonian $H(x) \in \mathbb{R}$ represents the total energy of the system and is supposed to be a sufficiently smooth function. A matrix $g(x,t) \in \mathbb{R}^{n\times m}$ represents the control port, and for all $x \in \mathbb{R}^n$ and $t \geqslant 0$, a skew-symmetric matrix $J(x,t) \in \mathbb{R}^{n\times n}$ represents the structure matrix and a symmetric positive semi-definite matrix $R_D(x,t) \in \mathbb{R}^{n\times n}$ represents the dissipation matrix. In what follows, an $n \times n$ positive (semi-) definite matrix A is represented by $A \succ 0_{n\times n}$ ($A \succeq 0_{n\times n}$), where $0_{n\times n}$ denotes the zero matrix of size $n \times n$.

According to the literature (Fujimito et al., 2003), we define a useful property called passivity for the port-Hamiltonian system (1), though this property can be defined for a more general input–output mapping (van der Schaft, 1996,). For a differentiable function $V(x,t)$ satisfying $V(x,t) \geqslant V(0_{n\times 1},t) = 0$, the system (1) is passive with respect to V if $\mathrm{d}V/\mathrm{d}t \leqslant y^\top u$ holds for all $x \in \mathbb{R}^n$ and $t \geqslant 0$. Note that as shown in (van der Schaft, 1996), a time-invariant port-Hamiltonian system with a positive semi-definite Hamiltonian is intrinsically passive with respect to its Hamiltonian. This comes from

$$\frac{\mathrm{d}H(x)}{\mathrm{d}t} = -\frac{\partial H(x)}{\partial x} R_D(x) \frac{\partial H(x)}{\partial x}^\top + \frac{\partial H(x)}{\partial x} g(x)u \leqslant y^\top u. \quad (2)$$

If the Hamiltonian is positive definite, Eq. (2) implies that a negative-feedback of the passive output, namely, $u = -Ky$ with a positive definite matrix $K \in \mathbb{R}^{m\times m}$ renders the origin of the system locally Lyapunov stable.

2.2. Generalized canonical transformations

In converting a positive semi-definite Hamiltonian into another positive definite one and performing coordinate and feedback transformations, the following result is helpful to designing such transformations while preserving the port-Hamiltonian structure. A generalized canonical transformation (Fujimito et al., 2003; Fujimito and Sugie, 2001) is the following set of transformations:

$$\begin{aligned} &\bar{x} = \Phi(x,t) \\ &\overline{H}(\bar{x},t) = H(x,t) + U(x,t)|_{x=\Phi^{-1}(\bar{x},t)} \\ &\bar{y} = y + \alpha(x,t)|_{x=\Phi^{-1}(\bar{x},t)} \\ &\bar{u} = u + \beta(x,t)|_{x=\Phi^{-1}(\bar{x},t)} \end{aligned} \quad (3)$$

such that the transformed system is another port-Hamiltonian system of the form (1) with the new state $\bar{x}$, Hamiltonian $\overline{H}$, output $\bar{y}$, and input $\bar{u}$. Here, a map $\Phi_t : \mathbb{R}^n \to \mathbb{R}^n$ defined as $\Phi_t(x) := \Phi(x,t) = \bar{x}$ is a diffeomorphism. In Eq. (3), we utilize the notation $\Phi^{-1}(\bar{x},t)$ as $\Phi_t^{-1}(\bar{x})$, that is, $\Phi^{-1}(\bar{x},t) = \Phi_t^{-1}(\bar{x}) = x$. Besides, a differentiable function $U : \mathbb{R}^n \times \mathbb{R} \to \mathbb{R}$ is a Hamiltonian transformation, and vector-valued functions $\alpha : \mathbb{R}^n \times \mathbb{R} \to \mathbb{R}^m$, and $\beta : \mathbb{R}^n \times \mathbb{R} \to \mathbb{R}^m$ are the output and input transformations, respectively.

The following theorem clarifies necessary and sufficient conditions for generalized canonical transformations:

Theorem 1. (Fujimito et al., 2003) Consider the port-Hamiltonian system (1). Necessary and sufficient conditions for the set of transformations (3) to be a generalized canonical transformation are as follows: There exist a skew-symmetric matrix $P_J(x,t) \in \mathbb{R}^{n\times n}$ and a symmetric matrix $Q_R(x,t) \in \mathbb{R}^{n\times n}$ such that $R_D(x,t) + Q_R(x,t)$ is pos-

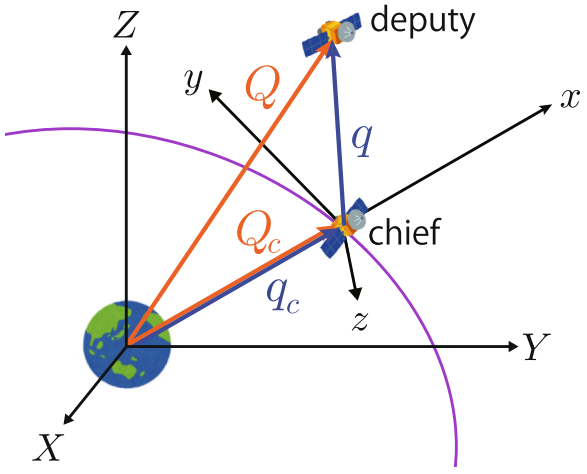

Fig. 1. ECI and LVLH frames.

itive semi-definite, and the following equations are satisfied:

$$-\frac{\partial \Phi}{\partial t}+\frac{\partial \Phi}{\partial x}\left[(J-R_D)\frac{\partial U}{\partial x}^{\top}+g\beta+(P_J-Q_R)\frac{\partial (H+U)}{\partial x}^{\top}\right]=0_{n\times 1}, \tag{4}$$

$$\alpha=g^{\top}\frac{\partial U}{\partial x}^{\top}. \tag{5}$$

Furthermore, when the transformed Hamiltonian satisfies $\overline{H}(\bar{x},t)\geqslant \overline{H}(0_{n\times 1},t)=0$, the transformed port-Hamiltonian system is passive with respect to $\overline{H}$ if and only if the following inequality holds:

$$-\frac{\partial (H+U)}{\partial t}+\frac{\partial (H+U)}{\partial x}\left[(J-R_D)\frac{\partial U}{\partial x}^{\top}+R_D\frac{\partial (H+U)}{\partial x}^{\top}+g\beta\right]\geqslant 0. \tag{6}$$

Remark 1. The condition in Eq. (6) is slightly different from the original one in Eq. (13) in (Fujimito et al., 2003) in that the original condition in (Fujimito et al., 2003) only provides a sufficient condition for passivity of the transformed system, while Eq. (6) in the present paper provides a necessary and sufficient condition.

3. Port-Hamiltonian representation of nonlinear relative orbital motion considering atmospheric drag

This study uses two coordinate frames: the ECI and LVLH frames depicted in Fig. 1. The ECI frame is an Earth-centered inertial frame. This frame takes the $X-Y$ plane as the equatorial plane and the origin as the center of the Earth, with the X axis in the direction of the vernal equinox, the Z axis in the direction of the north pole perpendicular to the equatorial plane, and the Y axis to form a right-handed orthogonal system. The LVLH frame is a chief-centered rotational frame. This frame takes the origin as a chief (a real satellite or a fictitious point), the x axis in the radial direction pointing from the center of the Earth to the chief, the z axis in the direction of the orbital angular momentum vector, and the y axis to form a right-handed orthogonal system.

Here, we describe the nonlinear relative orbital motion as a port-Hamiltonian system mentioned in Section 2.1, where we explicitly consider the gravitational J2 effect and atmospheric drag. In the ECI frame, the Lagrangian $\mathscr{L}$ is given by

$$\begin{aligned}\mathscr{L}(Q,\dot{Q}) &= \tfrac{1}{2}\dot{Q}^{\top}\dot{Q}-\mathscr{U}(Q)\\ &= \tfrac{1}{2}\dot{Q}^{\top}\dot{Q}-\left[-\tfrac{\mu}{\|Q\|}\left(1-\tfrac{J_2R_e^2}{2\|Q\|^2}\left(\tfrac{3Z^2}{\|Q\|^2}-1\right)\right)\right],\end{aligned} \tag{7}$$

where $Q:=(X,Y,Z)^{\top}\in\mathbb{R}^3$ denotes the position vector of the deputy and $\mathscr{U}(Q)\in\mathbb{R}$ denotes the gravitational potential including the effect of the J2 term with the gravitational constant of the Earth, μ [m^3/s^2], the radius of the Earth, R_e [m], and the J2 coefficient, J_2. Although this paper considers up to the J2 term, the proposed method can also handle potential functions including higher-order gravitational perturbations and those from other celestial bodies.

The coordinate transformation from the LVLH frame to the ECI frame for the position vector of the deputy is expressed as

$$Q=T(t)(q+q_c), \tag{8}$$

where $T(t)\in SO(3)$ represents the transformation matrix from the LVLH frame to the ECI frame. The LVLH frame can be expressed as a rotational sequence given by (Ω_c,i_c,θ_c) as the (3–1-3) Euler angles from the ECI frame, where Ω_c,i_c, and θ_c denote the right ascension of the ascending node, inclination, and argument of latitude of the chief, respectively. Therefore, the transformation matrix $T(t)$ in Eq. (8) is given by the following equation:

$$T(t)=\begin{bmatrix}\cos\Omega_c\cos\theta_c-\sin\Omega_c\sin\theta_c\cos i_c & -\cos\Omega_c\sin\theta_c-\sin\Omega_c\cos\theta_c\cos i_c & \sin\Omega_c\sin i_c\\ \sin\Omega_c\cos\theta_c+\cos\Omega_c\sin\theta_c\cos i_c & -\sin\Omega_c\sin\theta_c+\cos\Omega_c\cos\theta_c\cos i_c & -\cos\Omega_c\sin i_c\\ \sin\theta_c\sin i_c & \cos\theta_c\sin i_c & \cos i_c\end{bmatrix}.$$

In what follows, the argument (t) may be omitted from $T(t)$ for notational simplicity. It comes from Eq. (8) that

$$\dot{Q}=T(\dot{q}+\dot{q}_c+\omega^{\times}(q+q_c)), \tag{9}$$

where $\omega\in\mathbb{R}^3$ denotes the angular velocity of the LVLH frame to the ECI frame, and the relation for the time derivative of the rotational matrix, that is,

$$\frac{\mathrm{d}T(t)}{\mathrm{d}t}=T(t)\omega^{\times}$$

is used. Here, for a vector $\xi=[\xi_1,\xi_2,\xi_3]^{\top}\in\mathbb{R}^3$, a skew-symmetric matrix $\xi^{\times}\in\mathbb{R}^{3\times 3}$ is given by

$$\xi^{\times}=\begin{bmatrix}0 & -\xi_3 & \xi_2\\ \xi_3 & 0 & -\xi_1\\ -\xi_2 & \xi_1 & 0\end{bmatrix}.$$

Using the Lagrangian $\mathscr{L}$ calculated by Eqs. (7)–(9), the conjugate momentum $p\in\mathbb{R}^3$ corresponding to q is defined as

$$p := \frac{\partial \mathscr{L}}{\partial \dot{q}}^{\top} = \dot{q} + \dot{q}_c + \omega^{\times}(q + q_c). \tag{10}$$

The Legendre transformation leads to the Hamiltonian H as

$$H = \frac{1}{2}p^{\top}p - p^{\top}(\dot{q}_c + \omega^{\times}(q + q_c)) + \mathscr{U}(T(q + q_c)).$$

The atmospheric drag force in the LVLH frame is expressed as

$$\begin{aligned} f_{\text{Drag}} &= T^{\top}\left(-\tfrac{\rho_a A_C C_D}{2m_d}\|\dot{Q}\|\dot{Q}\right) \\ &= -r_{\text{Drag}}\|\dot{q} + v_{\text{ref}}\|(\dot{q} + v_{\text{ref}}) \\ &= -r_{\text{Drag}}\|\dot{q} + v_{\text{ref}}\|\left(\tfrac{\partial H(x,t)}{\partial p}^{\top} + v_{\text{ref}}\right), \end{aligned}$$

where the reference velocity $v_{\text{ref}} \in \mathbb{R}^3$ and the atmospheric drag coefficient $r_{\text{Drag}} \in \mathbb{R}$ are defined as

$$v_{\text{ref}} := \dot{q}_c + \omega^{\times}(q + q_c), \tag{11}$$

$$r_{\text{Drag}} := \frac{\rho_a A_C C_D}{2m_d}. \tag{12}$$

Here, we introduce the atmospheric drag matrix $\overline{R}_D \in \mathbb{R}^{3\times 3}$ as the following equation to represent the system with the atmospheric drag force f_{Drag} in a port-Hamiltonian system:

$$\overline{R}_D = r_{\text{Drag}}\|\dot{q} + v_{\text{ref}}\|I_3, \tag{13}$$

where I_m represents the identity matrix of size $m \times m$.

Finally, using the notation of $\overline{R}_D$ in Eq. (13), the nonlinear relative orbital motion considering the gravitational J2 effect and atmospheric drag in the LVLH frame is represented in a port-Hamiltonian system of the form (1) with an additional disturbance term as

$$\begin{bmatrix}\dot{q}\\ \dot{p}\end{bmatrix} = \begin{bmatrix}0_{m\times m} & I_m\\ -I_m & -\overline{R}_D\end{bmatrix}\begin{bmatrix}\frac{\partial H(x,t)}{\partial q}^{\top}\\ \frac{\partial H(x,t)}{\partial p}^{\top}\end{bmatrix} + \begin{bmatrix}0_{m\times m}\\ I_m\end{bmatrix}u_0 + \begin{bmatrix}0_{m\times 1}\\ -\overline{R}_D v_{\text{ref}}\end{bmatrix}, \tag{14}$$

$$y = \begin{bmatrix}0_{m\times m} & I_m\end{bmatrix}\begin{bmatrix}\frac{\partial H(x,t)}{\partial q}^{\top}\\ \frac{\partial H(x,t)}{\partial p}^{\top}\end{bmatrix} = \frac{\partial H(x,t)}{\partial p}^{\top} = \dot{q},$$

$$H(x,t) = \tfrac{1}{2}p^{\top}p - p^{\top}(\dot{q}_c + \omega^{\times}(q + q_c)) + \mathscr{U}(T(q + q_c))$$

with $m = 3$. Here, $u_0 \in \mathbb{R}^m$ is the control input and the state x consists of the position and conjugate momentum of the deputy as $x := (q^{\top}, p^{\top})^{\top} \in \mathbb{R}^{2m}$.

4. Construction of the error system based on generalized canonical transformations for reference trajectories

This section constructs an error system for a given reference formation trajectory that preserves the port-Hamiltonian structure and, moreover, possesses passivity using generalized canonical transformations. We first suppose that the atmospheric drag coefficient r_{Drag} in Eq. (12) is available for control. Then, in the next section, we present an adaptation mechanism provided that r_{Drag} is an unknown constant.

Let us define the control input u_0 to compensate for the disturbance due to the atmospheric drag, which appears as the last term on the right-hand side of Eq. (14) as follows:

$$u_0 = \overline{R}_D v_{\text{ref}} + u = r_{\text{Drag}}\|\dot{q} + v_{\text{ref}}\|v_{\text{ref}} + u, \tag{15}$$

where $u \in \mathbb{R}^m$ is a new control input. Substituting Eq. (15), Eq. (14) is rewritten as the following port-Hamiltonian system:

$$\begin{aligned} &\begin{bmatrix}\dot{q}\\ \dot{p}\end{bmatrix} = \begin{bmatrix}0_{m\times m} & I_m\\ -I_m & -\overline{R}_D\end{bmatrix}\begin{bmatrix}\frac{\partial H(x,t)}{\partial q}^{\top}\\ \frac{\partial H(x,t)}{\partial p}^{\top}\end{bmatrix} + \begin{bmatrix}0_{m\times m}\\ I_m\end{bmatrix}u \\ &y = \begin{bmatrix}0_{m\times m} & I_m\end{bmatrix}\begin{bmatrix}\frac{\partial H(x,t)}{\partial q}^{\top}\\ \frac{\partial H(x,t)}{\partial p}^{\top}\end{bmatrix} = \frac{\partial H(x,t)}{\partial p}^{\top} = \dot{q} \\ &H(x,t) = \tfrac{1}{2}p^{\top}p - p^{\top}(\dot{q}_c + \omega^{\times}(q + q_c)) + \mathscr{U}(T(q + q_c)). \end{aligned} \tag{16}$$

Then, we provide the following theorem for the concrete construction of the error system using the generalized canonical transformation for the port-Hamiltonian system expressed in Eq. (16):

Theorem 2. Consider the port-Hamiltonian system (16) and any twice differentiable reference trajectory q^d. The following set of transformations converts the system into the error system for q^d:

$$\begin{aligned} \Phi(x,t) &= \begin{bmatrix} T(t)(q - q^d) \\ p - (\dot{q}^d + \dot{q}_c + \omega^{\times}(q^d + q_c))\end{bmatrix} = \begin{bmatrix}\bar{q}\\ \bar{p}\end{bmatrix} \\ U(x,t) &= p^{\top}(-\dot{q}^d + \omega^{\times}(q - q^d)) - \mathscr{U}(T(t)(q + q_c)) \\ &\quad + \tfrac{1}{2}(\dot{q}^d + \dot{q}_c + \omega^{\times}(q^d + q_c))^{\top} \\ &\quad (\dot{q}^d + \dot{q}_c + \omega^{\times}(q^d + q_c)) \\ \alpha(x,t) &= -\dot{q}^d + \omega^{\times}(q - q^d) \\ \beta(x,t) &= -\ddot{q}^d - \ddot{q}_c - \omega^{\times}(\dot{q}^d + \dot{q}_c) - \dot{\omega}^{\times}(q^d + q_c) \\ &\quad -\omega^{\times}p - \tfrac{\partial \mathscr{U}(T(t)(q+q_c))}{\partial q}^{\top} - \overline{R}_D\{\dot{q}^d - \omega^{\times}(q - q^d)\}. \end{aligned} \tag{17}$$

The transformed error system is given as the following another port-Hamiltonian system:

$$\begin{aligned} &\begin{bmatrix}\dot{\bar{q}}\\ \dot{\bar{p}}\end{bmatrix} = \begin{bmatrix}0_{m\times m} & T(t)\\ -T(t)^{\top} & -\overline{R}_D\end{bmatrix}\begin{bmatrix}\frac{\partial \overline{H}(\bar{x})}{\partial \bar{q}}^{\top}\\ \frac{\partial \overline{H}(\bar{x})}{\partial \bar{p}}^{\top}\end{bmatrix} + \begin{bmatrix}0_{m\times m}\\ I_m\end{bmatrix}\bar{u} \\ &\bar{y} = \begin{bmatrix}0_{m\times m} & I_m\end{bmatrix}\begin{bmatrix}\frac{\partial \overline{H}(\bar{x})}{\partial \bar{q}}^{\top}\\ \frac{\partial \overline{H}(\bar{x})}{\partial \bar{p}}^{\top}\end{bmatrix} = \frac{\partial \overline{H}(\bar{x})}{\partial \bar{p}}^{\top} = \bar{p} \\ &\overline{H}(\bar{x}) = \tfrac{1}{2}\bar{p}^{\top}\bar{p}. \end{aligned} \tag{18}$$

Furthermore, the resultant error system is passive for the new input–output pair $(\bar{u}, \bar{y})$ with respect to the new Hamiltonian $\overline{H}$.

Proof. First, we check that the set of transformations (17) satisfies the necessary and sufficient conditions for generalized canonical transformations in Theorem 1. Suppose $P_J = Q_R = 0_{m\times m}$, the left-hand side of Eq. (4) can be calculated using Eq. (17) as follows:

$$
\begin{aligned}
&-\begin{bmatrix} T\omega^{\times}(q-q^d)-T\dot{q}^d \\ -\ddot{q}^d-\ddot{q}_c-\omega^{\times}(\dot{q}^d+\dot{q}_c)-\dot{\omega}^{\times}(q^d+q_c)) \end{bmatrix} \\
&+\begin{bmatrix} T & 0_{m\times m} \\ 0_{m\times m} & I_m \end{bmatrix}\left\{\begin{bmatrix} 0_{m\times m} & I_m \\ -I_m & -\overline{R}_D \end{bmatrix}\right. \\
&\times\begin{bmatrix} -\omega^{\times}p-\frac{\partial \mathscr{U}(T(t)(q+q_c))^{\top}}{\partial q} \\ -\dot{q}^d+\omega^{\times}(q-q^d) \end{bmatrix} \\
&+\left.\begin{bmatrix} 0_{m\times 1} \\ -\ddot{q}^d-\ddot{q}_c-\omega^{\times}(\dot{q}^d+\dot{q}_c)-\dot{\omega}^{\times}(q^d+q_c)-\omega^{\times}p \\ -\frac{\partial \mathscr{U}(T(t)(q+q_c))^{\top}}{\partial q}-\overline{R}_D\{\dot{q}^d-\omega^{\times}(q-q^d)\} \end{bmatrix}\right\} \\
&=\begin{bmatrix} 0_{m\times 1} \\ 0_{m\times 1} \end{bmatrix}.
\end{aligned}
$$

Thus, the condition of Eq. (4) is shown to hold. The second condition (5) is verified by comparing $\alpha(x,t)$ in Eq. (17) with the right-hand side of Eq. (5) as

$$
\begin{aligned}
g^{\top}\frac{\partial U^{\top}}{\partial x} &= [\,0_{m\times m} \quad I_m\,]\begin{bmatrix} -\omega^{\times}p-\frac{\partial \mathscr{U}^{\top}}{\partial q} \\ -\dot{q}^d+\omega^{\times}(q-q^d) \end{bmatrix} \\
&= -\dot{q}^d+\omega^{\times}(q-q^d).
\end{aligned}
$$

Therefore, the set of transformations (17) is a generalized canonical transformation.

Next, we confirm the passivity condition in Eq. (6) for the transformed system. It comes from Eqs. (16) and (17) that

$$
\begin{aligned}
H+U &= \tfrac{1}{2}p^{\top}p-p^{\top}(\dot{q}_c+\omega^{\times}(q+q_c)) \\
&\quad +\mathscr{U}(T(q+q_c))+p^{\top}(-\dot{q}^d+\omega^{\times}(q-q^d)) \\
&\quad -\mathscr{U}(T(q+q_c))+\tfrac{1}{2}(\dot{q}^d+\dot{q}_c+\omega^{\times}(q^d+q_c))^{\top} \\
&\quad (\dot{q}^d+\dot{q}_c+\omega^{\times}(q^d+q_c)) \\
&= \tfrac{1}{2}p^{\top}p+\tfrac{1}{2}(\dot{q}^d+\dot{q}_c+\omega^{\times}(q^d+q_c))^{\top} \\
&\quad (\dot{q}^d+\dot{q}_c+\omega^{\times}(q^d+q_c))-p^{\top}(\dot{q}^d+\dot{q}_c+\omega^{\times}(q^d+q_c)) \\
&= \tfrac{1}{2}(p-(\dot{q}^d+\dot{q}_c+\omega^{\times}(q^d+q_c)))^{\top} \\
&\quad (p-(\dot{q}^d+\dot{q}_c+\omega^{\times}(q^d+q_c))).
\end{aligned} \tag{19}
$$

From Eq. (19), we have

$$
\begin{aligned}
&-\tfrac{\partial(H+U)}{\partial t}+\tfrac{\partial(H+U)}{\partial x}\left\{(J-R_D)\tfrac{\partial U^{\top}}{\partial x}+g\beta\right\} \\
&= -(p-(\dot{q}^d+\dot{q}_c+\omega^{\times}(q^d+q_c)))^{\top} \\
&\quad (-\ddot{q}^d-\ddot{q}_c-\omega^{\times}(\dot{q}^d+\dot{q}_c)-\dot{\omega}^{\times}(q^d+q_c)) \\
&\quad +\begin{bmatrix} 0_{m\times 1} \\ p-(\dot{q}^d+\dot{q}_c+\omega^{\times}(q^d+q_c)) \end{bmatrix}^{\top} \\
&\quad \left\{\begin{bmatrix} 0_{m\times m} & I_m \\ -I_m & -\overline{R}_D \end{bmatrix}\begin{bmatrix} -\omega^{\times}p-\frac{\partial \mathscr{U}^{\top}}{\partial q} \\ -\dot{q}^d+\omega^{\times}(q-q^d) \end{bmatrix}\right. \\
&\quad \left.+\begin{bmatrix} 0_{m\times 1} \\ -\ddot{q}^d-\ddot{q}_c-\omega^{\times}(\dot{q}^d+\dot{q}_c)-\dot{\omega}^{\times}(q^d+q_c) \\ -\omega^{\times}p-\frac{\partial \mathscr{U}}{\partial q}^{\top}+\overline{R}_D(-\dot{q}^d+\omega^{\times}(q-q^d)) \end{bmatrix}\right\} \\
&= -(p-(\dot{q}^d+\dot{q}_c+\omega^{\times}(q^d+q_c)))^{\top} \\
&\quad (-\ddot{q}^d-\ddot{q}_c-\omega^{\times}(\dot{q}^d+\dot{q}_c)-\dot{\omega}^{\times}(q^d+q_c)) \\
&\quad +\begin{bmatrix} 0_{m\times 1} \\ p-(\dot{q}^d+\dot{q}_c+\omega^{\times}(q^d+q_c)) \end{bmatrix}^{\top} \\
&\quad \begin{bmatrix} -\dot{q}^d+\omega^{\times}(q-q^d) \\ -\ddot{q}^d-\ddot{q}_c-\omega^{\times}(\dot{q}^d+\dot{q}_c)-\dot{\omega}^{\times}(q^d+q_c) \end{bmatrix} \\
&= 0.
\end{aligned} \tag{20}
$$

Consequently, using Eq. (20), we can show that

$$
\begin{aligned}
\text{The left-hand side of Eq. (6)} &= \tfrac{\partial(H+U)}{\partial x}R_D\tfrac{\partial(H+U)}{\partial x}^{\top} \\
&\geqslant 0.
\end{aligned}
$$

Now, we confirm that the transformed system is an error system. From the definition of the transformation in Eq. (17), it follows that $q=q^d$ when $\bar{x}=0$, because $\bar{q}=0$ and T is non-singular. In addition to the result $q=q^d$, Eq. (10) leads to the fact $\dot{q}=\dot{q}^d$ under $\bar{p}=0$. Hence, $\bar{x}=0$ implies that $q=q^d$ and $\dot{q}=\dot{q}^d$. Conversely, when $q=q^d$ and $\dot{q}=\dot{q}^d$, it comes from Eq. (17) that $\bar{x}=0$.

Finally, to show that the transformed system is a port-Hamiltonian system described by Eq. (18). We calculate the dynamics of the transformed system as

$$
\begin{aligned}
\begin{bmatrix} \dot{\bar{q}} \\ \dot{\bar{p}} \end{bmatrix} &= \tfrac{\partial\Phi}{\partial t}+\tfrac{\partial\Phi}{\partial x}\dot{x} \\
&= \begin{bmatrix} T\omega^{\times}(q-q^d)-T\dot{q}^d \\ -\ddot{q}^d-\ddot{q}_c-\omega^{\times}(\dot{q}^d+\dot{q}_c)-\dot{\omega}^{\times}(q^d+q_c) \end{bmatrix} \\
&\quad +\begin{bmatrix} T & 0_{m\times m} \\ 0_{m\times m} & I_m \end{bmatrix}\left\{\begin{bmatrix} 0_{m\times m} & I_m \\ -I_m & -\overline{R}_D \end{bmatrix}\begin{bmatrix} \frac{\partial H}{\partial q}^{\top} \\ \frac{\partial H}{\partial p}^{\top} \end{bmatrix}+\begin{bmatrix} 0_{m\times m} \\ I_m \end{bmatrix}u\right\}.
\end{aligned} \tag{21}
$$

Substituting $u=\bar{u}-\beta$ into Eq. (21) with β from Eq. (17), we obtain the following equation:

$$
\begin{aligned}
\begin{bmatrix} \dot{\bar{q}} \\ \dot{\bar{p}} \end{bmatrix} &= \begin{bmatrix} T\{p-(\dot{q}^d+\dot{q}_c+\omega^{\times}(q^d+q_c))\} \\ \bar{u}-\overline{R}_D\{p-(\dot{q}^d+\dot{q}_c+\omega^{\times}(q^d+q_c))\} \end{bmatrix} \\
&= \begin{bmatrix} T\bar{p} \\ \bar{u}-\overline{R}_D\bar{p} \end{bmatrix}.
\end{aligned} \tag{22}
$$

Besides, noting that the new Hamiltonian is given by $\overline{H}(\bar{x})=1/2\bar{p}^{\top}\bar{p}$, the right-hand side of Eq. (18) can be calculated as

$$
\begin{aligned}
&\begin{bmatrix} 0_{m\times m} & T \\ -T^{\top} & -\overline{R}_D \end{bmatrix}\begin{bmatrix} \frac{\partial \overline{H}(\bar{x})}{\partial \bar{q}}^{\top} \\ \frac{\partial \overline{H}(\bar{x})}{\partial \bar{p}}^{\top} \end{bmatrix}+\begin{bmatrix} 0_{m\times m} \\ I_m \end{bmatrix}\bar{u} \\
&= \begin{bmatrix} 0_{m\times m} & T \\ -T^{\top} & -\overline{R}_D \end{bmatrix}\begin{bmatrix} 0_{m\times 1} \\ \bar{p} \end{bmatrix}+\begin{bmatrix} 0_{m\times 1} \\ \bar{u} \end{bmatrix} \\
&= \begin{bmatrix} T\bar{p} \\ \bar{u}-\overline{R}_D\bar{p} \end{bmatrix}
\end{aligned} \tag{23}
$$

It comes from Eqs. (22) and (23) that the dynamics of the transformed system is described by Eq. (18). Next, the transformed output is calculated as

$$\begin{aligned}\bar{y} &= y + \alpha \\ &= [\,0_{m\times m} \quad I_m\,]\tfrac{\partial H}{\partial x}^\top + [\,0_{m\times m} \quad I_m\,]\tfrac{\partial U}{\partial x}^\top \\ &= [\,0_{m\times m} \quad I_m\,]\tfrac{\partial (H+U)}{\partial x}^\top.\end{aligned}$$

Also, using the fact that

$$\begin{aligned}\tfrac{\partial (H+U)}{\partial x} &= \tfrac{\partial \overline{H}(\bar{x})}{\partial \bar{x}}\tfrac{\partial \Phi(x)}{\partial x} \\ &= \tfrac{\partial \overline{H}(\bar{x})}{\partial \bar{x}}\begin{bmatrix} T & 0_{m\times m} \\ 0_{m\times m} & I_m \end{bmatrix} \\ &= \left[\tfrac{\partial \overline{H}}{\partial \bar{q}}T, \quad \tfrac{\partial \overline{H}}{\partial \bar{p}}\right],\end{aligned}$$

the output satisfies the following relation:

$$\bar{y} = [\,0_{m\times m} \quad I_m\,]\begin{bmatrix} T^\top \tfrac{\partial \overline{H}}{\partial \bar{q}}^\top \\ \tfrac{\partial \overline{H}}{\partial \bar{p}}^\top \end{bmatrix} = \frac{\partial \overline{H}}{\partial \bar{p}}^\top. \tag{24}$$

Thus, Eq. (24) shows that the transformed output is consistent with Eq. (18). This completes the proof. □

5. Trajectory tracking control with an adaptive mechanism for unknown atmospheric drag coefficient

In this section, we treat the atmospheric drag coefficient as an unknown constant and propose a trajectory tracking controller with an adaptive mechanism to estimate the atmospheric drag coefficient.

First, we define an estimated atmospheric drag matrix $\widehat{R}_D$ using the estimated atmospheric drag coefficient $\hat{r}_{\mathrm{Drag}}$ similarly to Eq. (13) as

$$\widehat{R}_D = \hat{r}_{\mathrm{Drag}}\|\dot{q} + v_{\mathrm{ref}}\|I_m. \tag{25}$$

The estimation error for the unknown constant r_{Drag} is defined as

$$\tilde{r}_{\mathrm{Drag}} := \hat{r}_{\mathrm{Drag}} - r_{\mathrm{Drag}}.$$

Now, we replace the true coefficient with the estimated one in the compensation input in Eq. (15) as

$$u_0 = \widehat{R}_D v_{\mathrm{ref}} + u = \hat{r}_{\mathrm{Drag}}\|\dot{q} + v_{\mathrm{ref}}\|v_{\mathrm{ref}} + u. \tag{26}$$

Then, the system corresponding to Eq. (16) becomes the following port-Hamiltonian system with the disturbance term due to the estimation error of the atmospheric drag coefficient:

$$\begin{aligned}&\begin{bmatrix}\dot{q}\\ \dot{p}\end{bmatrix} = \begin{bmatrix} 0_{m\times m} & I_m \\ -I_m & -\overline{R}_D \end{bmatrix}\begin{bmatrix}\tfrac{\partial H(x,t)}{\partial q}^\top \\ \tfrac{\partial H(x,t)}{\partial p}^\top\end{bmatrix} \\ &+\begin{bmatrix}0_{m\times m}\\ I_m\end{bmatrix}u + \begin{bmatrix}0_{m\times 1}\\ \tilde{r}_{\mathrm{Drag}}\|\dot{q} + v_{\mathrm{ref}}\|v_{\mathrm{ref}}\end{bmatrix} \\ &y = [\,0_{m\times m} \quad I_m\,]\begin{bmatrix}\tfrac{\partial H(x,t)}{\partial q}^\top \\ \tfrac{\partial H(x,t)}{\partial p}^\top\end{bmatrix} = \tfrac{\partial H(x,t)}{\partial p}^\top = \dot{q} \\ &H(x,t) = \tfrac{1}{2}p^\top p - p^\top(\dot{q}_c + \omega^\times(q+q_c)) + \mathscr{U}(T(q+q_c)).\end{aligned} \tag{27}$$

Accordingly, the generalized canonical transformation presented in Eq. (17) is now modified as

$$\begin{aligned}\Phi(x,t) &= \begin{bmatrix} T(t)(q-q^d) \\ p - (\dot{q}^d + \dot{q}_c + \omega^\times(q^d + q_c))\end{bmatrix} = \begin{bmatrix}\bar{q}\\ \bar{p}\end{bmatrix} \\ U(x,t) &= p^\top(-\dot{q}^d + \omega^\times(q-q^d)) - \mathscr{U}(T(t)(q+q_c)) \\ &+\tfrac{1}{2}(\dot{q}^d + \dot{q}_c + \omega^\times(q^d+q_c))^\top(\dot{q}^d + \dot{q}_c + \omega^\times(q^d+q_c)) \\ \alpha(x,t) &= -\dot{q}^d + \omega^\times(q-q^d) \\ \beta(x,t) &= -\ddot{q}^d - \ddot{q}_c - \omega^\times(\dot{q}^d + \dot{q}_c) - \dot{\omega}^\times(q^d+q_c) \\ &-\omega^\times p - \tfrac{\partial \mathscr{U}(T(t)(q+q_c))}{\partial q}^\top - \widehat{R}_D\{\dot{q}^d - \omega^\times(q-q^d)\}.\end{aligned} \tag{28}$$

Using the generalized canonical transformation (28) for the system (27), we obtain the following error system:

$$\begin{aligned}&\begin{bmatrix}\dot{\bar{q}}\\ \dot{\bar{p}}\end{bmatrix} = \begin{bmatrix} 0_{m\times m} & T \\ -T^\top & -\overline{R}_D\end{bmatrix}\begin{bmatrix}\tfrac{\partial \overline{H}(\bar{x})}{\partial \bar{q}}^\top \\ \tfrac{\partial \overline{H}(\bar{x})}{\partial \bar{p}}^\top\end{bmatrix} + \begin{bmatrix}0_{m\times m}\\ I_m\end{bmatrix}\bar{u} \\ &+\begin{bmatrix}0_{m\times 1}\\ \tilde{r}_{\mathrm{Drag}}\|\dot{q} + v_{\mathrm{ref}}\|(\dot{q}^d + \dot{q}_c + \omega^\times(q^d+q_c))\end{bmatrix} \\ &\bar{y} = [\,0_{m\times m} \quad I_m\,]\begin{bmatrix}\tfrac{\partial \overline{H}(\bar{x})}{\partial \bar{q}}^\top \\ \tfrac{\partial \overline{H}(\bar{x})}{\partial \bar{p}}^\top\end{bmatrix} = \tfrac{\partial \overline{H}(\bar{x})}{\partial \bar{p}}^\top = \bar{p} \\ &\overline{H}(\bar{x}) = \tfrac{1}{2}\bar{p}^\top\bar{p}.\end{aligned} \tag{29}$$

Finally, we show the following theorem that provides a stabilizing controller for the error system (29), an adaptive update law for the atmospheric drag coefficient, and a theoretical guarantee for the closed-loop system:

Theorem 3. Suppose that the orbital angular velocity vector of the chief ω is bounded and any twice differentiable reference trajectory q^d. Consider the error system in Eq. (29), and the following control input with symmetric positive definite matrices $K_p, K_d \in \mathbb{R}^{m\times m}$:

$$\begin{aligned}\bar{u} &= -T^\top\tfrac{\partial \overline{U}(\bar{q})}{\partial \bar{q}}^\top - K_d\tfrac{\partial \overline{H}(\bar{x})}{\partial \bar{p}}^\top \\ &= -T^\top K_p\bar{q} - K_d\bar{p}\end{aligned} \tag{30}$$

with a potential function defined as

$$\overline{U}(\bar{q}) = \frac{1}{2}\bar{q}^\top K_p\bar{q}. \tag{31}$$

The closed-loop system is given by

$$\begin{aligned}&\begin{bmatrix}\dot{\bar{q}}\\ \dot{\bar{p}}\end{bmatrix} = \begin{bmatrix} 0_{m\times m} & T \\ -T^\top & -(K_d + \overline{R}_D)\end{bmatrix}\begin{bmatrix}\tfrac{\partial \widehat{H}(\bar{x})}{\partial \bar{q}}^\top \\ \tfrac{\partial \widehat{H}(\bar{x})}{\partial \bar{p}}^\top\end{bmatrix} \\ &+\begin{bmatrix}0_{m\times 1}\\ \tilde{r}_{\mathrm{Drag}}\|\dot{q} + v_{\mathrm{ref}}\|(\dot{q}^d + \dot{q}_c + \omega^\times(q^d+q_c))\end{bmatrix}, \\ &\widehat{H}(\bar{x}) = \frac{1}{2}\bar{p}^\top\bar{p} + \overline{U}(\bar{q}).\end{aligned} \tag{32}$$

Also, consider the following adaptive update law for the estimated atmospheric drag coefficient:

$$\dot{\hat{r}}_{\mathrm{Drag}} = -k_r\|\dot{q}+v_{\mathrm{ref}}\|\left(\bar{p}^\top+\kappa\bar{q}^\top T\right) \times\left(\dot{q}^d+\dot{q}_c+\omega^\times\left(q^d+q_c\right)\right), \tag{33}$$

where k_r and κ are positive constants.

Then, κ can be chosen small enough so that $\left[\bar{x}^\top,\ \tilde{r}_{\mathrm{Drag}}\right]^\top = 0_{(2m+1)\times 1}$ becomes an uniformly Lyapunov stable equilibrium point, and furthermore, the following convergence property holds:

$$\lim_{t\to\infty}\bar{x}(t) = 0_{2m\times 1}.$$

Proof. The closed-loop system in Eq. (32) is straightforwardly verified by substituting Eqs. (30) and (31) into Eq. (29) and utilizing the relation that $\partial\overline{H}/\partial\bar{p} = \partial\widehat{H}/\partial\bar{p}$.

Let us define a Lyapunov function candidate as follows:

$$\begin{aligned} E\left(\bar{x},\tilde{r}_{\mathrm{Drag}},t\right) &:= \widehat{H}(\bar{x}) + \kappa\bar{q}^\top T(t)\bar{p} + \tfrac{1}{2k_r}\tilde{r}_{\mathrm{Drag}}^2 \\ &= \tfrac{1}{2}\bar{p}^\top\bar{p} + \tfrac{1}{2}\bar{q}^\top K_p\bar{q} + \kappa\bar{q}^\top T(t)\bar{p} + \tfrac{1}{2k_r}\tilde{r}_{\mathrm{Drag}}^2 \\ &= \tfrac{1}{2}\begin{bmatrix}\bar{q}^\top & \bar{p}^\top\end{bmatrix}\begin{bmatrix}K_p & \kappa T(t)\\ \kappa T(t)^\top & I_m\end{bmatrix}\begin{bmatrix}\bar{q}\\ \bar{p}\end{bmatrix} + \tfrac{1}{2k_r}\tilde{r}_{\mathrm{Drag}}^2, \end{aligned} \tag{34}$$

where the positive constant κ satisfies the following equation:

$$0 < \kappa < \min\left\{1,\ \sqrt{\lambda_{\min}\left(K_p\right)}\right\}. \tag{35}$$

Here, $\lambda_{\min}(\cdot)$ and $\lambda_{\max}(\cdot)$ represent the minimum and maximum eigenvalues of the argument, respectively. It comes from Schur's lemma that

$$\begin{bmatrix}K_p & \kappa T\\ \kappa T^\top & I_m\end{bmatrix} \succ 0 \quad\Longleftrightarrow\quad K_p - \kappa^2 TT^\top = K_p - \kappa^2 I_m \succ 0. \tag{36}$$

Since κ is chosen to satisfy Eq. (35), $K_p-\kappa^2 I_m$ is a positive definite matrix. Thus, from Eqs. (36) and (34), $E\left(\bar{x},\tilde{r}_{\mathrm{Drag}},t\right)$ is a positive definite function with respect to $\left(\bar{x},\tilde{r}_{\mathrm{Drag}}\right)$ for $\forall t\geqslant 0$. Furthermore, the following inequalities with respect to the function $E\left(\bar{x},\tilde{r}_{\mathrm{Drag}},t\right)$ hold:

$$\begin{aligned} &\frac{1-\kappa}{2}\bar{p}^\top\bar{p} + \frac{1}{2}\bar{q}^\top\left(K_p-\kappa I_m\right)\bar{q} + \frac{1}{2k_r}\tilde{r}_{\mathrm{Drag}}^2 \leqslant E\left(\bar{x},\tilde{r}_{\mathrm{Drag}},t\right) \\ &\quad\leqslant \frac{1+\kappa}{2}\bar{p}^\top\bar{p} + \frac{1}{2}\bar{q}^\top\left(K_p+\kappa I_m\right)\bar{q} + \frac{1}{2k_r}\tilde{r}_{\mathrm{Drag}}^2. \end{aligned} \tag{37}$$

Since the leftmost function in Eq. (37) is also a positive definite function with respect to $\left(\bar{x},\tilde{r}_{\mathrm{Drag}}\right)$ from Eq. (35), $E\left(\bar{x},\tilde{r}_{\mathrm{Drag}},t\right)$ is bounded from above and below by a time-invariant positive definite function, as shown by Eq. (37).

Using Eq. (33), the time derivative of the Lyapunov function candidate E along the solution to the closed-loop system in Eq. (32) is calculated as follows:

$$\begin{aligned} \dot{E} &= \tfrac{\partial E}{\partial t} + \tfrac{\partial E}{\partial\bar{x}}\dot{\bar{x}} + \tfrac{\partial E}{\partial\tilde{r}_{\mathrm{Drag}}}\dot{\tilde{r}}_{\mathrm{Drag}} \\ &= \kappa\bar{q}^\top\dot{T}\bar{p} + \begin{bmatrix}\frac{\partial E(\bar{x},t)}{\partial\bar{q}} & \frac{\partial E(\bar{x},t)}{\partial\bar{p}}\end{bmatrix}\begin{bmatrix}\dot{\bar{q}}\\ \dot{\bar{p}}\end{bmatrix} + \tfrac{\tilde{r}_{\mathrm{Drag}}}{k_r}\dot{\tilde{r}}_{\mathrm{Drag}} \\ &= \kappa\bar{q}^\top T\omega^\times\bar{p} + \begin{bmatrix}\frac{\partial\widehat{H}(\bar{x})}{\partial\bar{q}} + \kappa\bar{p}^\top T^\top & \frac{\partial\widehat{H}(\bar{x})}{\partial\bar{p}} + \kappa\bar{q}^\top T\end{bmatrix} \\ &\quad\left\{\begin{bmatrix}0_{m\times m} & T\\ -T^\top & -\left(K_d+\overline{R}_D\right)\end{bmatrix}\begin{bmatrix}\frac{\partial\widehat{H}(\bar{x})}{\partial\bar{q}}^\top\\ \frac{\partial\widehat{H}(\bar{x})}{\partial\bar{p}}^\top\end{bmatrix}\right. \\ &\quad\left.+\begin{bmatrix}0_{m\times 1}\\ \tilde{r}_{\mathrm{Drag}}\|\dot{q}+v_{\mathrm{ref}}\|\left(\dot{q}^d+\dot{q}_c+\omega^\times\left(q^d+q_c\right)\right)\end{bmatrix}\right\} + \tfrac{\tilde{r}_{\mathrm{Drag}}}{k_r}\dot{\tilde{r}}_{\mathrm{Drag}} \\ &= \kappa\bar{q}^\top T\omega^\times\bar{p} - \tfrac{\partial\widehat{H}}{\partial\bar{p}}\left(K_d+\overline{R}_D\right)\tfrac{\partial\widehat{H}}{\partial\bar{p}}^\top \\ &\quad+\begin{bmatrix}-\kappa\bar{q}^\top TT^\top & \kappa\bar{p}^\top T^\top T - \kappa\bar{q}^\top T\left(K_d+\overline{R}_D\right)\end{bmatrix}\begin{bmatrix}\frac{\partial\widehat{H}(\bar{x})}{\partial\bar{q}}^\top\\ \frac{\partial\widehat{H}(\bar{x})}{\partial\bar{p}}^\top\end{bmatrix} \\ &\quad+\begin{bmatrix}\bar{q}^\top K_p + \kappa\bar{p}^\top T^\top & \bar{p}^\top + \kappa\bar{q}^\top T\end{bmatrix} \\ &\quad\begin{bmatrix}0_{m\times 1}\\ \tilde{r}_{\mathrm{Drag}}\|\dot{q}+v_{\mathrm{ref}}\|\left(\dot{q}^d+\dot{q}_c+\omega^\times\left(q^d+q_c\right)\right)\end{bmatrix} \\ &\quad+\tfrac{\tilde{r}_{\mathrm{Drag}}}{k_r}\left(-k_r\|\dot{q}+v_{\mathrm{ref}}\|\left(\bar{p}^\top+\kappa\bar{q}^\top T\right)\left(\dot{q}^d+\dot{q}_c+\omega^\times\left(q^d+q_c\right)\right)\right) \\ &= \kappa\bar{q}^\top T\omega^\times\bar{p} - \bar{p}^\top\left(K_d+\overline{R}_D\right)\bar{p} - \kappa\bar{q}^\top K_p\bar{q} \\ &\quad+\kappa\bar{p}^\top\bar{p} - \kappa\bar{q}^\top T\left(K_d+\overline{R}_D\right)\bar{p} \\ &\quad\leqslant -\lambda_{\min}\left(K_d+\overline{R}_D\right)\|\bar{p}\|^2 - \kappa\lambda_{\min}\left(K_p\right)\|\bar{q}\|^2 + \kappa\|\bar{p}\|^2 \\ &\quad+\kappa\|T\|\left(\|\omega^\times\| + \lambda_{\max}\left(K_d+\overline{R}_D\right)\right)\|\bar{q}\|\|\bar{p}\| \end{aligned}$$

From the assumption that $\omega(t)$ is bounded, we define

$$\omega_{\max} := \sup_{t\geqslant 0}\|\omega(t)\| < \infty, \tag{38}$$

and since $T\in SO(3)$, we have $\|T\| = 1$. In addition, for any $a\in\mathbb{R}^3$, $\|a^\times\| = \|a\|$ holds. Therefore, by applying Young's inequality with ϵ as an arbitrary positive constant, the following inequality holds:

$$\begin{aligned} \dot{E} &\leqslant -\lambda_{\min}\left(K_d+\overline{R}_D\right)\|\bar{p}\|^2 - \kappa\lambda_{\min}\left(K_p\right)\|\bar{q}\|^2 \\ &\quad+\kappa\|\bar{p}\|^2 + \kappa\left(\omega_{\max}+\lambda_{\max}\left(K_d+\overline{R}_D\right)\right)\left(\tfrac{\epsilon\|\bar{q}\|^2}{2} + \tfrac{\|\bar{p}\|^2}{2\epsilon}\right) \\ &= -\kappa\left\{\lambda_{\min}\left(K_p\right) - \tfrac{\epsilon\left(\omega_{\max}+\lambda_{\max}\left(K_d+\overline{R}_D\right)\right)}{2}\right\}\|\bar{q}\|^2 \\ &\quad-\left\{\lambda_{\min}\left(K_d+\overline{R}_D\right) - \kappa\left(1+\tfrac{\omega_{\max}+\lambda_{\max}\left(K_d+\overline{R}_D\right)}{2\epsilon}\right)\right\}\|\bar{p}\|^2. \end{aligned} \tag{39}$$

For Eq. (39), we can always choose $\epsilon > 0$ such that

$$\begin{aligned} &\lambda_{\min}\left(K_p\right) - \frac{\epsilon\left(\omega_{\max}+\lambda_{\max}\left(K_d+\overline{R}_D\right)\right)}{2} > 0 \\ &\quad\Longleftrightarrow\quad 0 < \epsilon < \frac{2\lambda_{\min}\left(K_p\right)}{\omega_{\max}+\lambda_{\max}\left(K_d+\overline{R}_D\right)}. \end{aligned} \tag{40}$$

Moreover, for any ϵ satisfying Eq. (40), there always exists κ that satisfies the following equation:

$$\lambda_{\min}\left(K_d+\overline{R}_D\right)-\kappa\left(1+\frac{\omega_{\max}+\lambda_{\max}\left(K_d+\overline{R}_D\right)}{2\epsilon}\right)>0\iff\kappa<\frac{\lambda_{\min}\left(K_d+\overline{R}_D\right)}{1+\frac{\omega_{\max}+\lambda_{\max}\left(K_d+\overline{R}_D\right)}{2\epsilon}}. \tag{41}$$

Combining the conditions in (35) and (41) that κ must satisfy, we can always find κ such that

$$0<\kappa<\min\left\{1,\ \sqrt{\lambda_{\min}\left(K_p\right)},\ \frac{\lambda_{\min}\left(K_d+\overline{R}_D\right)}{1+\frac{\omega_{\max}+\lambda_{\max}\left(K_d+\overline{R}_D\right)}{2\epsilon}}\right\}. \tag{42}$$

Hence, according to Eqs. (39), (40), and (42), it has been shown that there exists a time-invariant and continuous positive definite function $W(\bar{x})$ with respect to $\bar{x}$ satisfying the following equation:

$$\dot{E}\leqslant -W(\bar{x}). \tag{43}$$

From Eq. (43), $\left[\bar{x}^\top,\ \tilde{r}_{\mathrm{Drag}}\right]^\top=0_{(2m+1)\times 1}$ in the closed-loop system is endowed with uniform Lyapunov stability. Furthermore, since it comes from generalized LaSalle's theorem (Theorem 5.27 in (Sastry, 1999)) that

$$\lim_{t\to\infty}W(\bar{x})=0,$$

it has been shown that the following convergence property holds:

$$\lim_{t\to\infty}\bar{x}(t)=0_{2m\times 1}.$$

This completes the proof. □

Finally, using Eqs. (3), (26), (28), and (30), the trajectory tracking controller for the system (27) is summarized as follows:

$$\begin{aligned}u_0=&-T^\top K_pT(q-q^d)-K_d(p-\dot{q}^d-\dot{q}_c-\omega^\times(q^d+q_c))\\&+\ddot{q}^d+\ddot{q}_c+\omega^\times(\dot{q}^d+\dot{q}_c)+\dot{\omega}^\times(q^d+q_c)\\&+\omega^\times p+\tfrac{\partial\mathcal{W}(T(q+q_c))}{\partial q}^\top+\widehat{R}_D(\dot{q}^d+\dot{q}_c+\omega^\times(q^d+q_c)).\end{aligned} \tag{44}$$

6. Simulation results

This section shows simulation results to demonstrate the validity of the proposed method. In this simulation, the reference formation configuration for two deputy satellites is a GCO with a radius ρ of 50 m to maintain a straight formation with a relative distance of 100 m. The control objective of this simulation is set to reduce the relative distance error between satellites to the order of 10^{-3} mm for possible future precision formation control. We give the reference trajectory q_i^d for the ith deputy ($i\in\{1,2\}$) as follows:

$$q_i^d=\begin{bmatrix}\frac{1}{2}\rho\sin(n_ct+\phi_i)\\ \rho\cos(n_ct+\phi_i)\\ \frac{\sqrt{3}}{2}\rho\sin(n_ct+\phi_i)\end{bmatrix}, \tag{45}$$

where $\phi_i=(i-1)\pi$ [rad] and n_c is the mean motion of the chief and is equal to $\left(\mu/a_c^3\right)^{1/2}$, where a_c [m] is the semi-major axis of the chief. The orbital elements of the chief are set as follows:

$$a_c=6.928142\times 10^6\mathrm{m},\quad e_c=0,\quad i_c=98^\circ,\quad \theta_c=30^\circ.$$

The true coefficient r_{Drag} in Eq. (12) is set to 1.415683×10^{-12}, where a small satellite with a mass of 180 kg is assumed and the atmospheric density value is determined as the average of the atmospheric densities at an altitude of 550 km that are in the top 7% in each year during 2001–2021, using the Jacchia–Bowman 2008 model.

We set the initial position error of each deputy to 0.25 m (0.5%) and replace ρ for deputies 1 and 2 in Eq. (45) with 1.005ρ and 0.995ρ, respectively. We suppose a precise micro-thruster system as the actuator, and the control input is continuously variable acceleration. In addition, the maximum output norm of the acceleration is limited to 2.5×10^{-6} m/s^2, where the basis for the micro-thruster is the existing throttleable propulsion system in (Noci et al., 2009). We parameterize the design parameters of the controller in Eq. (30) with a positive constant k_p,

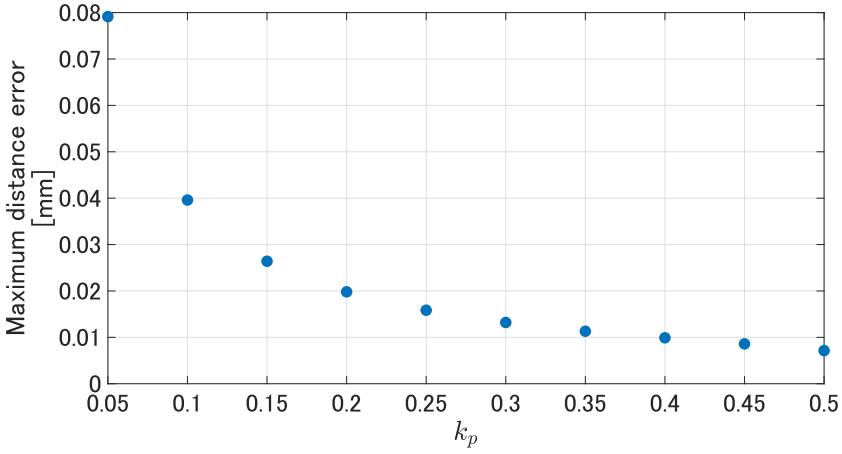

Fig. 2. Maximum distance error between the deputies at the 3rd revolution.

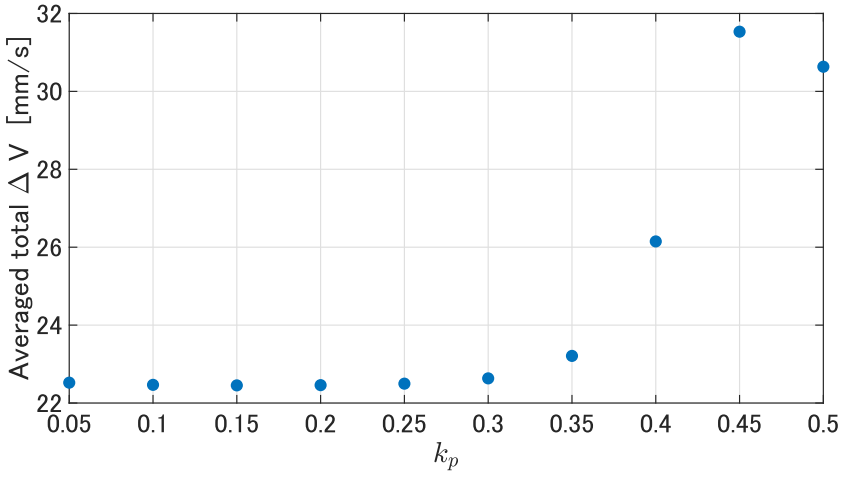

Fig. 3. Averaged total ΔV of two deputies for three revolutions.

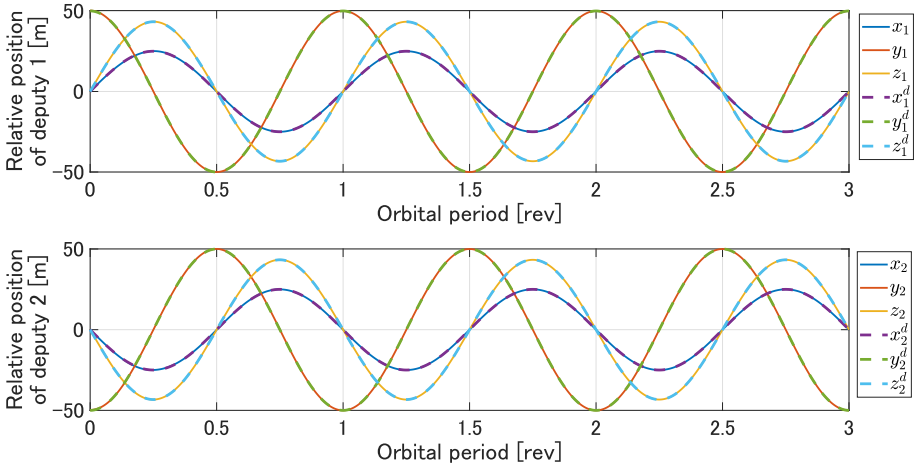

Fig. 4. Time responses of the relative position of two deputies ($k_p = 0.5$).

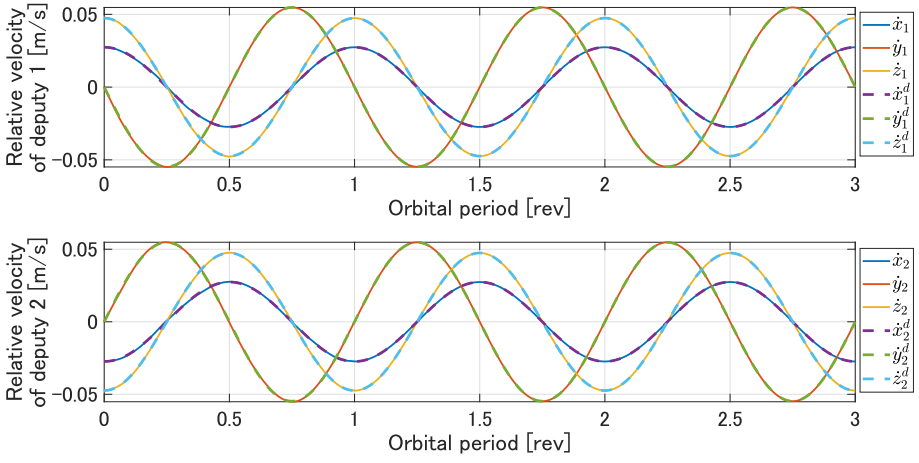

Fig. 5. Time responses of the relative velocity of two deputies ($k_p = 0.5$).

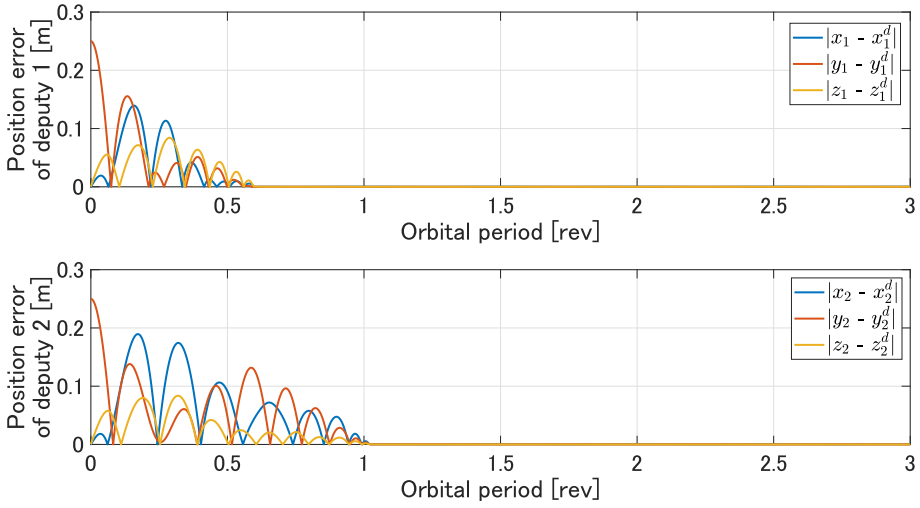

Fig. 6. Tracking errors of the position of two deputies ($k_p = 0.5$).

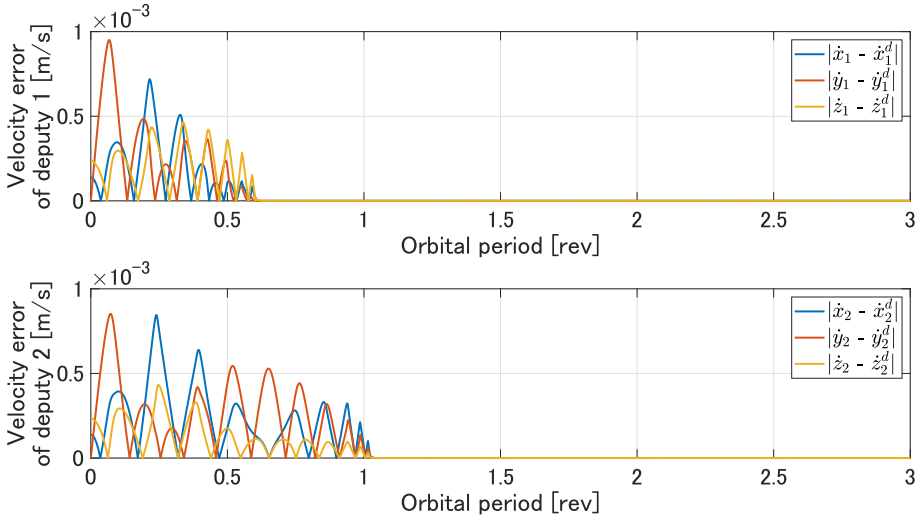

Fig. 7. Tracking errors of the velocity of two deputies ($k_p = 0.5$).

namely, the positive definite symmetric matrices K_p and K_d are parameterized as

$$K_p = k_p I_3, \quad K_d = 30 k_p I_3. \tag{46}$$

The rest parameters of the adaptive mechanism in Eq. (33) are set to $k_r = 1.0 \times 10^{-12}$ and $\kappa = 5.0 \times 10^{-2}$.

The simulations are performed using a 4th-order Runge–Kutta method, setting the time step size and control period to 0.2 s and the number of revolutions around the Earth to 3. Simulation results are presented from Figs. 2–10. Fig. 2 shows the maximum error of the distance between the deputies at the 3rd revolution when k_p in Eq. (46) is varied in 0.05 increments, from 0.05 to 0.5. Fig. 3 shows the average of the sum of ΔV of two deputies for three revolutions when k_p is varied under the same condition, where ΔV represents the velocity change indicating fuel consumption.

In the following, time responses when k_p is fixed at 0.5 are exhibited, which corresponds to the case with the smallest maximum distance error between the deputies. Figs. 4 and 5 show the time responses of the relative position and velocity of each deputy from the chief. The solid lines represent the state of each deputy, and the dotted lines represent the reference trajectory of each deputy. To quantify the errors in tracking to the reference trajectories, Figs. 6 and 7 show the time transition of the norm of the position and velocity errors. Fig. 8 shows the time responses of the control input of each deputy summarized in Eq. (44) and its norm, respectively.

Fig. 9 shows the time transition of the estimated atmospheric drag coefficient $\hat{r}_{\mathrm{Drag}}$ in the solid line, where the dotted line represents the true coefficient r_{Drag}. This figure implies that the estimate of each deputy remains bounded and converges to a constant value.

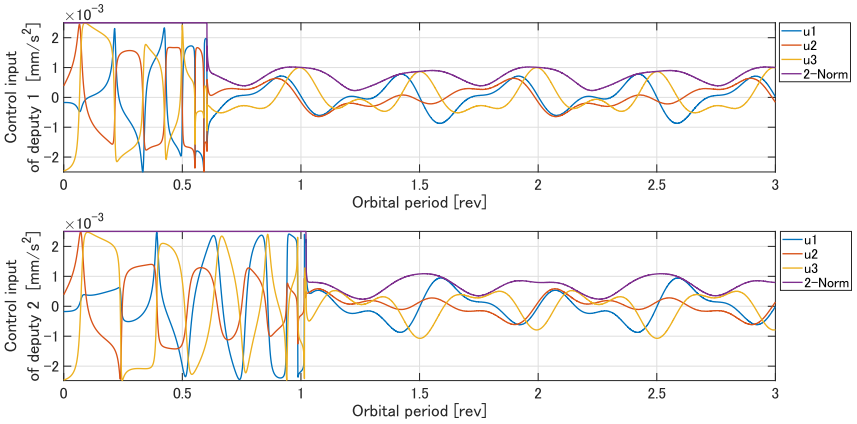

Fig. 8. Time responses of control input and its norm of two deputies ($k_p = 0.5$).

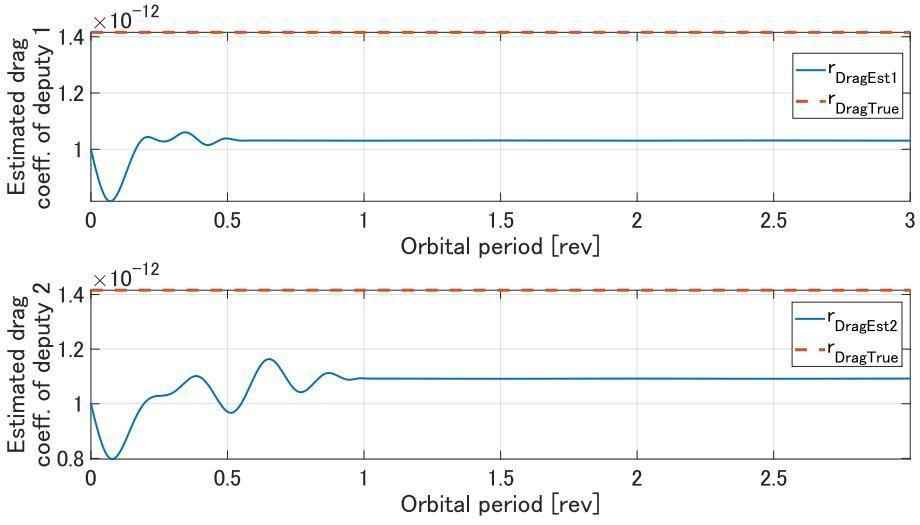

Fig. 9. Time transition of the estimated atmospheric drag coefficient ($k_p = 0.5$).

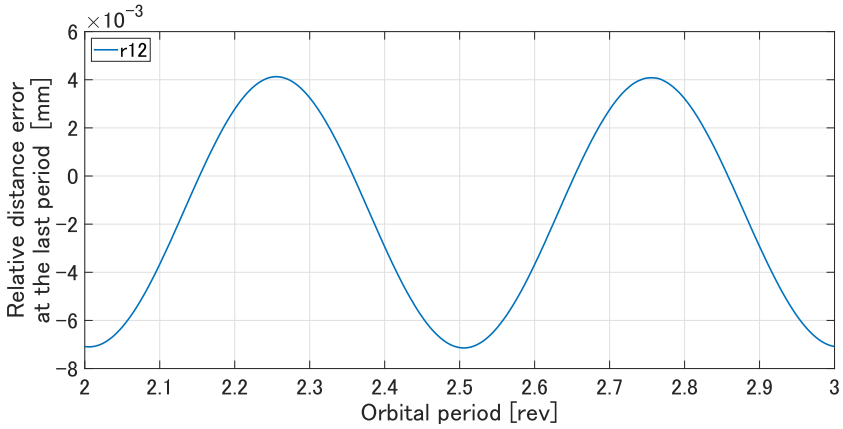

Fig. 10. Time transition of the relative distance error between the deputies at the last period ($k_p = 0.5$).

Lastly, to quantify the accuracy of the formation shape, Fig. 10 shows the time transition of the relative distance error between the deputies at the last period. This figure indicates that we can achieve the formation control accuracy on the order of 10^{-3} mm. Consequently, these figures confirm that the deputies follow their reference formation

trajectories while estimating the unknown atmospheric drag coefficient and achieve the desired formation accurately.

Comparing the proposed method with Ref. (Tabuchi et al., 2022), the comparison method can achieve a smaller maximum distance error by selecting the gain parameter, while the averaged ΔV becomes larger. When comparing the averaged ΔV required for one revolution under the same control accuracy, Ref. (Tabuchi et al., 2022) is more than twice that of the proposed method. The proposed method enables efficient control with the same level of control accuracy.

7. Conclusion

This paper proposes a nonlinear formation tracking control method using generalized canonical transformations with an adaptive mechanism for an unknown atmospheric drag. First, a port-Hamiltonian representation of the nonlinear relative orbital motion with the gravitational J2 and atmospheric drag effects is modeled. Second, a specific construction of an error system for any twice differentiable reference formation trajectory using generalized canonical transformations is constructed. Third, a passivity-based asymptotic stabilizing controller and an adaptive mechanism for the error system are presented. The proposed method stabilizes the error system based on its passivity while updating the estimate of the atmospheric drag coefficient. Consequently, it is guaranteed that the estimation error of the atmospheric drag coefficient is bounded and that the tracking error for the reference trajectory converges uniformly asymptotically to zero. The effectiveness of the proposed method is demonstrated through numerical simulations.

The proposed method can handle any differentiable potential functions and twice differentiable reference trajectories; hence, gravitational perturbations of arbitrary complexity and various formation and transition/escape trajectories can be handled in a unified manner. Furthermore, the proposed method does not impose any linearizations, and thus, it can be applied to long-distance and ultra-precise formations necessary for future formation flying space interferometer missions.

Since the main focus of the present study is to develop a framework for theoretical assurance of asymptotic stability of the entire control system, the atmospheric drag coefficient is supposed to be an unknown constant. In future work, we will extend the proposed method to the time-varying case by applying model reference adaptive control.

Declaration of competing interest

The authors declare that they have no known competing financial interests or personal relationships that could have appeared to influence the work reported in this paper.

Acknowledgment

This work was partially supported by JSPS KAKENHI Grant No. JP24K00909.

References

Acosta, J., Ortega, R., Astolfi, A., et al., 2005. Interconnection and damping assignment passivity-based control of mechanical systems with underactuation degree one. IEEE Trans. Autom. Contr. 50 (12), 1936–1955. https://doi.org/10.1016/S1474-6670(17)31354-X.

Alfriend, K.T., Vadali, S.R., Gurfil, P., et al., 2010. Spacecraft formation flying: dynamics, control and navigation. Butterworth-Heinemann. https://doi.org/10.1016/C2009-0-17485-8.

Bassetto, M., Mengali, G., Quarta, A.A., 2024. Drag sail attitude tracking via nonlinear control. Acta Astronaut. 225, 845–856. https://doi.org/10.1016/j.actaastro.2024.09.046.

Clohessy, W.H., Wiltshire, R.S., 1960. Terminal guidance system for satellite rendezvous. J. Aerospace Sci. 27 (9), 653–658. https://doi.org/10.2514/8.8704.

D'Amico, S., Montenbruck, O., 2006. Proximity operations of formation-flying spacecraft using an eccentricity/inclination vector separation. J. Guid., Control, Dynam. 29 (3), 554–563. https://doi.org/10.2514/1.15114.

Danzmann, K., Rüdiger, A., 2003. LISA technology-concept, status, prospects. Class. Quant. Grav. 20 (10), S1–S9. https://doi.org/10.1088/0264-9381/20/10/301.

Duindam, V., Macchelli, A., Stramigioli, S. et al., Eds., 2009. Modeling and Control of Complex Physical Systems: The Port-Hamiltonian Approach. Springer-Verlag, Berlin. doi:10.1007/978-3-642-03196-0.

Ferguson, J., Donaire, A., Middleton, R.H., 2019. Kinetic-potential energy shaping for mechanical systems with applications to tracking. IEEE Control Syst. Lett. 3 (4), 960–965. https://doi.org/10.1109/LCSYS.2019.2919842.

Fu, X., Xu, M., 2019. Formation flying along low-energy lunar transfer trajectory using Hamiltonian-structure-preserving control. J. Guid., Control, and Dynam. 42 (3), 650–661. https://doi.org/10.2514/1.G003673.

Fujimito, K., Sakurama, K., Sugie, T., 2003. Trajectory tracking control of port-controlled Hamiltonian systems via generalized canonical transformations. Automatica 39 (12), 2059–2069. https://doi.org/10.1016/j.automatica.2003.07.005.

Fujimito, K., Sugie, T., 2001. Canonical transformation and stabilization of generalized Hamiltonian systems. Syst. Control Lett. 42 (3), 217–227. https://doi.org/10.1016/S0167-6911(00)00091-8.

Hamanaka, Y., Satoh, S., 2023. Formation tracking control based on generalized canonical transformation with adaptive mechanism for atmospheric drag. In: Proc. 34th Int. Symp. Space Technology and Science (pp. 2023–d–16).

Hill, G.W., 1878. Researches in the Lunar theory. Am. J. Math. 1, 5–26. https://doi.org/10.2307/2369430.

Hui, L., Li, J., 2009. Terminal sliding mode control for spacecraft formation flying. IEEE Trans. Aerospace Electron. Syst. 45 (3), 835–846. https://doi.org/10.1109/TAES.2009.5259168.

Itkis, U., 1976. Control Systems of Variable Structure. Wiley, New York.

Ito, T., 2024. Formation-flying interferometry in geocentric orbits. Astron. Astrophys. 682, A38. https://doi.org/10.1051/0004-6361/202348218.

Ito, T., Izumi, K., Kawano, I. et al., 2025. SILVIA: Ultra-precision formation flying demonstration for space-based interferometry. Publicat. Astron. Soc. Japan, p. psaf086. doi:10.1093/pasj/psaf086.

Ito, T., Kawano, I., Funaki, I., et al., 2021. Utilizing low Earth orbit for a space interferometer laboratory by three satellites. Proc. 11th Int. ESA Conf. Guidance, Navigation & Control Systems.

Javanmardi, N., Yaghmaei, A., Yazdanpanah, M.J., 2020. Spacecraft formation flying in the port-hamiltonian framework. Nonlinear Dyn. 99, 2765–2783. https://doi.org/10.1007/s11071-019-05445-0.

Kawamura, S. et al., 2008. The Japanese space gravitational wave antenna - DECIGO. J. Phys.: Conf. Ser. 122, 012006. https://doi.org/10.1088/1742-6596/122/1/012006.

Khalil, H.K., 1996. Nonlinear Systems, 3rd ed. Macmillan Publishing Company, New York.

Lawn, M., Ton, C., Baldwin, M., 2018. Spacecraft formation flying using sliding mode control with nonsingular terminal sliding surface. Proc. American Control Conf., 6138–6143 https://doi.org/10.23919/ACC.2018.8431381.

Li, Q., Yuan, J., Wang, H., 2018. Sliding mode control for autonomous spacecraft rendezvous with collision avoidance. Acta Astronaut. 151, 743–751. https://doi.org/10.1016/j.actaastro.2018.07.006.

Llorente, J., Agenjo, A., Carrascosa, C., et al., 2013. PROBA-3: precise formation flying demonstration mission. Acta Astronaut. 82 (1), 38–46.

Maschke, B., van der Schaft, A.J., 1992. Port-controlled hamiltonian systems: modelling origins and system theoretic properties. In: Proc. 2nd IFAC Symp. Nonlinear Control Systems, pp. 282–288. https://doi.org/10.1016/S1474-6670(17)52308-3.

Matsuo, T., Ikari, S., Kondo, H., et al., 2022. High spatial resolution spectral imaging method for space interferometers and its application to formation flying small satellites. J. Astron. Telescopes, Instrum., Syst. 8 (1), 015001. https://doi.org/10.1117/1.JATIS.8.1.015001.

Mauro, G.D., Lawn, M., Bevilacqua, R., 2018. Survey on guidance navigation and control requirements for spacecraft formation-flying missions. J. Guid., Control, Dynam. 41 (3), 581–602. https://doi.org/10.2514/1.G002868.

Molina, I.V., Delpech, M., Delong, N., et al., 2024. POC_ESSAIM: close-formation flying demonstration of 3 nanosatellites in LEO. In: Proc. 29th Int. Symp. Space Flight Dynamics.

Noci, G., Matticari, G., Siciliano, P., et al., 2009. Cold gas micro propulsion system for scientific satellite fine pointing: review of development and qualification activities at thales alenia space italia. In: 45th AIAA/ASME/SAE/ASEE Joint Propulsion Conference & Exhibit. https://doi.org/10.2514/6.2009-5127.

Ohkami, Y., Kawano, I., 2003. Autonomous rendezvous and docking by engineering test satellite VII: a challenge of Japan in guidance, navigation and control –Breakwell memorial lecture. Acta Astronaut. 53 (1), 1–8. https://doi.org/10.1016/S0094-5765(02)00195-9.

Ortega, R., van der Schaft, A.J., Maschke, B., et al., 2002. Interconnection and damping assignment passivity-based control of port-controlled Hamiltonian systems. Automatica 38 (4), 585–596. https://doi.org/10.1016/S0005-1098(01)00278-3.

Quanz, S.P., Ottiger, M., Fontanet, E. et al., 2022. Large interferometer for exoplanets (LIFE) - I. Improved exoplanet detection yield estimates for a large mid-infrared space-interferometer mission. Astron. Astrophys., 664, A21. doi:10.1051/0004-6361/202140366.

Sastry, S., 1999. Nonlinear Systems: Anaysis, Stability and Control volume 10 of Interdisciplinary Applied Mathematics. Springer-Verlag, New York. doi:10.1007/978-1-4757-3108-8.

Satoh, S., 2021. Passivity based tracking control for spacecraft formation flying using generalized canonical transformations. In: Proc. SICE Multi-symposium on Control Systems (pp. 3D2–6). (in Japanese).

Scharf, D., Hadaegh, F., Ploen, S., 2004. A survey of spacecraft formation flying guidance and control (part 2): control. Proc. American Control Conf., 2976–2985 https://doi.org/10.23919/ACC.2004.1384365.

Schaub, H., Junkins, J.L., 2018. Analytical Mechanics of Space Systems, 4th ed. AIAA, Reston, VA.

Scheeres, D.J., Hsiao, F.Y., Vinh, N.X., 2003. Stabilizing motion relative to an unstable orbit: applications to spacecraft formation flight. J. Guid., Control, Dynam. 26 (1), 62–73. https://doi.org/10.2514/2.5015.

Serrano, D., Scoarnec, Y., Riveras, S.T., et al., 2025. Proba-3 Precise formation flying: an in-flight reality now. In: Proc. 76th International Astronautical Congress (p. Paper ID: 101648).

Shtessel, Y., Edwards, C., Fridman, L., et al., 2013. Sliding Mode Control and Observation. Birkhäeuser, New York. https://doi.org/10.1007/978-0-8176-4893-0.

Tabuchi, I., Satoh, S., Yamada, K., 2022. Formation tracking control using generalized canonical transformations and sliding mode control of port-Hamiltonian systems. In: Proc. 33rd Int. Symp. Space Technology and Science (pp. 2022–d–46).

van der Schaft, A.J., 1996. L_2-gain and Passivity Techniques in Nonlinear Control, volume 218. Lecture Notes on Control and Information Science, Berlin. https://doi.org/10.1007/978-3-319-49992-5.

Xie, X., Jiang, F., Li, J., 2024. Low frequency hierarchical cooperative impulse control for gravitational wave detector formation keeping. J. Guid., Control, Dynam., 1–15 https://doi.org/10.2514/1.G007932.